Saturation behavior of a one-pump fiber optical parametric amplifier in the presence of the fourth-order dispersion coefficient and dispersion fluctuation

N. Othman[1,*], K. G. Tay[1,], N. S. Mohd Shah[2], R. Talib[1], H. Pakarzadeh[3], and N. A. Cholan[1]**

[1]*Faculty of Electrical and Electronic Engineering, Universiti Tun Hussein Onn Malaysia, 86400 Batu Pahat, Johor, Malaysia*

[2]*Faculty of Engineering Technology, Universiti Tun Hussein Onn Malaysia, 84600 Pagoh, Johor, Malaysia*

[3]*Department of Physics, Shiraz University of Technology, Shiraz, Iran*

**Corresponding author: nurulanatiothman@gmail.com; **corresponding author: tay@uthm.edu.my*

Received April 16, 2019; accepted June 26, 2019; posted online September 4, 2019

The influence of the fourth-order dispersion coefficient on the behavior of parametric gain and saturation power of a one-pump fiber optical parametric amplifier over a signal wavelength span in the presence of fiber random dispersion fluctuations was investigated. The output signal power for the parametric gain calculation was obtained by numerically solving the three-coupled amplitude equations. Based on the calculations of the parametric gain over a variation of the signal wavelength, it is found that the saturation power behavior is dependent on the behavior of parametric gain. The manipulations of signal wavelength and the fourth-order dispersion coefficient changed the phase-matching condition, thereby affecting the resulting parametric gain and saturation power.

OCIS codes: 060.4370, 230.2285, 190.4380, 260.2030.
doi: 10.3788/COL201917.110603.

A fiber optical parametric amplifier (FOPA) is a device that utilizes the nonlinear effect of four-wave mixing (FWM). FWM is a type of optical third-order Kerr nonlinearity[1]. Besides FOPA, the FWM effect has also been adopted in other devices such as filters[2], optical generators[3], and wavelength converters[4]. The use of the FWM effect in FOPA has made it surpass the abilities of two major conventional amplifiers, i.e., Raman amplifier (RA) and erbium-doped fiber amplifier (EDFA). An FOPA is able to provide adjustable gain spectra and center frequency, as well as a 0 dB noise figure, which cannot be offered by the RA and EDFA[5].

One of the important parameters of an FOPA is its parametric gain. Theoretically, the input signal power of the FOPA plays an important role in determining the parametric gain. The FOPA with small input signal power is most likely to have high parametric gain[6]. In contrast, a lower parametric gain is usually attained when a high input signal power is used. The reduction of parametric gain when the high input signal power is used indicates that the parametric gain is saturating[7]. The parametric gain saturates at a different value of input signal power, and the value is dependent on the signal wavelength of FOPA[8]. The behavior of the parametric gain in the saturation regime (i.e., high input signal power) has been reported in various works[8–10]. Nevertheless, only particular signal wavelengths were selected for the saturation analysis. In this work, the saturation behavior was analyzed for a wide range of signal wavelengths. This work is especially beneficial for applications that require FOPA to operate in the saturation regime. Among the related applications are signal regeneration[11,12] and noise suppression[13]. Therefore, it is useful to know the saturation power at each signal wavelength in order to fulfill the requirement of the application.

The saturation power is determined by the input signal power at which 3 dB reduction of parametric gain from its initial value occurs. This means that the performance of parametric gain contributes to the saturation power behavior. The performance of FOPA parametric gain, especially at the signal wavelength far from the pump wavelength is influenced by the fourth-order dispersion coefficient, β_4 of the optical fiber[10,14,15]. Hence, it is much more accurate to include β_4 while investigating the behavior of saturation power over signal wavelength.

This Letter, thus, presents a numerical simulation of saturation power on one-pump (1-P) FOPA with the influence of β_4 of highly nonlinear dispersion-shifted fiber (HNL-DSF). The behavior of parametric gain and saturation power over a signal wavelength span was investigated for different values of β_4. In the simulation work, fiber random dispersion fluctuations were taken into account, alongside pump depletion and fiber losses. The random dispersion fluctuations are vital to be taken into account, as in practice their existence cannot be avoided.

In a 1-P FOPA, the FWM process, which is based on a parametric process, is adopted. The parametric process is a process in which the pump power is transferred to the signal and idler waves. The idler is a new generated wave at frequency ω_i, and its generation is due to the

propagation of the pump (at frequency ω_p) and signal (at frequency ω_s) throughout the fiber length. Interactions between the pump, signal, and idler waves are represented by the three-coupled amplitude equations, such that[16]

$$\frac{\mathrm{d}A_p}{\mathrm{d}z} = i\gamma\left\{A_p\left[|A_p|^2 + 2\left(|A_s|^2 + |A_i|^2\right)\right]\right\} + 2i\gamma A_s A_i A_p^* \exp(i\Delta\beta z) - \frac{1}{2}\alpha A_p, \tag{1}$$

$$\frac{\mathrm{d}A_s}{\mathrm{d}z} = i\gamma\left\{A_s\left[|A_s|^2 + 2\left(|A_p|^2 + |A_i|^2\right)\right]\right\} + i\gamma A_p^2 A_i^* \exp(-i\Delta\beta z) - \frac{1}{2}\alpha A_s, \tag{2}$$

$$\frac{\mathrm{d}A_i}{\mathrm{d}z} = i\gamma\left\{A_i\left[|A_i|^2 + 2\left(|A_p|^2 + |A_s|^2\right)\right]\right\} + i\gamma A_p^2 A_s^* \exp(-i\Delta\beta z) - \frac{1}{2}\alpha A_i, \tag{3}$$

where A_p, A_s, and A_i are the pump, signal, and idler amplitudes, respectively; meanwhile, * denotes their complex conjugates. γ and α represent fiber nonlinearity and losses, correspondingly. The linear phase-mismatch $\Delta\beta$ along the fiber length z is expressed as

$$\Delta\beta = \left\{\beta_2 + \frac{\beta_4}{2}\left[(\omega_p - \omega_0)^2 + \frac{1}{6}(\omega_p - \omega_s)^2\right]\right\} \cdot (\omega_p - \omega_s)^2 + \delta\beta, \tag{4}$$

in terms of second-order (β_2) and fourth-order (β_4) dispersion coefficients, as well as random dispersion fluctuations $\delta\beta$. ω_0 denotes the zero-dispersion frequency such as $\omega_0 = 2\pi c/\lambda_0$, where λ_0 is the zero-dispersion wavelength (ZDW) of the optical fiber.

The random fluctuations are modeled by following Gaussian distribution, such as $\delta\beta = \sigma \times n$, where n is a normal distribution in the range of $[-1, 1]$, and σ is the standard deviation[17]. σ is also known as the fluctuation amplitude, which is expressed as $\sigma = f\gamma P_{p0}$, where f and P_{p0} denote a dimensionless physical constant and input pump power, correspondingly. Along the fiber length L, the random variation of $\delta\beta$ was assumed as a piecewise constant with a correlation length L_c, and L_c is the average length scale over which the fluctuations take place[9]. In simulation work, a fiber will be divided into N segments, such as $N = L/L_c$, and, over each segment, the fluctuation was fixed. The length of each segment can be computed by $z = -L_c \times \ln n$[9].

In $\delta\beta$ modeling, it can be observed that σ and L_c will affect the phase-matching condition and, thus, the performance of 1-P FOPA. In Refs. [9,10], the effect of σ and L_c variations on the amplifier performance was investigated. Generally, it was reported that the effect of high σ and short L_c of $\delta\beta$ is more severe than the effect of low σ and long L_c. This was demonstrated by the reduction of parametric gain when σ is increased and L_c is reduced.

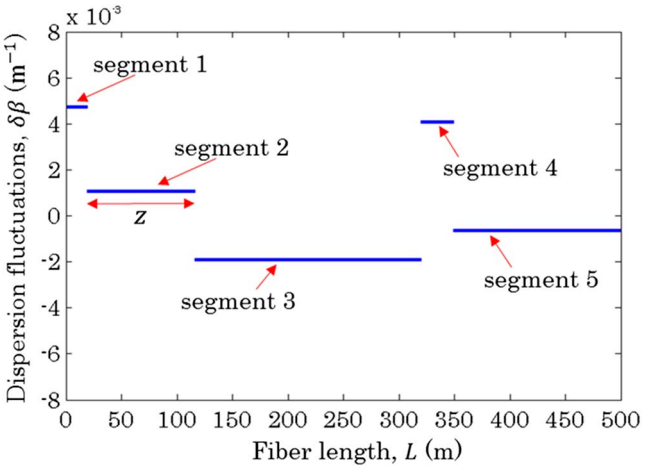

Fig. 1. Random dispersion fluctuations with $\sigma = 0.5\gamma P_{p0}$ and $L_c = 100$ m.

In this Letter, $\delta\beta$ is modeled with $\sigma = 0.5\gamma P_{p0}$ and $L_c = 100$ m. These values provide the average effect of dispersion fluctuations on the 1-P FOPA performance. In this simulation work, a short HNL-DSF, of which the length was about 500 m, was used to avoid broken phase-matching, which usually occurs in a long fiber[18]. The nonlinearity and losses of the HNL-DSF are $\gamma = 11.5\ \mathrm{W}^{-1} \cdot \mathrm{km}^{-1}$ and $\alpha = 0.82$ dB/km, respectively. An example of the $\delta\beta$ pattern when $P_{p0} = 30$ dBm is shown in Fig. 1. As seen, the number of segment $N = 5$ for $L_c = 100$ m with fiber length $L = 500$ m. The $\sigma = 0.5\gamma P_{p0}$ represents the average range of $\delta\beta$ between each segment. The range of $\delta\beta$ will be increased as the value of σ increases, hence making the fluctuations more pronounced.

As for parametric gain, the calculation was realized by numerically solving Eqs. (1)–(3) using the Runge–Kutta–Fehlberg method, with $A_{j0} = \sqrt{P_{j0}}$ for $j \in \{p, s, i\}$ as the input values for the first segment. The Runge–Kutta method was chosen because it offers stable numerical results[19]. The outputs of the first segment were then used as the inputs for the second segment, and again the equations were solved. The computation was repeated for the next segment and terminated once the outputs of the last segment were acquired. For the calculation of parametric gain G, the output signal power P_s of the last segment was divided with the input signal power P_{s0} such as $G = 10\log(P_s/P_{s0})$ (in dB)[7]. Owing to the stochastic nature of the dispersion fluctuations, the following computation process was repeated for a large number of $\delta\beta$ patterns with similar values of σ and L_c. Eventually, upon completing calculations for each $\delta\beta$, the average parametric gain $\bar{G}$ was computed. All computations were conducted in MATLAB software.

In this simulation work, the investigation of saturation power at different signal wavelengths λ_s was simulated with parameters $L = 500$ m, $\alpha = 0.82$ dB/km, $\gamma = 11.5\ \mathrm{W}^{-1} \cdot \mathrm{km}^{-1}$, $\lambda_0 = 1556.5$ nm, and $\beta_2 = -1.97 \times 10^{-2}\ \mathrm{ps}^2/\mathrm{km}$. Meanwhile, $P_{p0} = 30$ dBm at wavelength $\lambda_p = 1558$ nm, and input signal power is within the range

of $P_{s0} = -40$ to 20 dBm at each signal wavelength λ_s in the gain spectrum. The effect of signal wavelength on saturation power was simulated for three different values of β_4, i.e., $\beta_4 = 0$, 3.03×10^{-5}, and 6.23×10^{-5} ps^4/km[10]. The saturation power was determined by reducing the parametric gain 3 dB from its initial value in the small-signal regime. As an example, in Fig. 2(a), the parametric gain for $\beta_4 = 6.23 \times 10^{-5}$ ps^4/km with $\delta\beta$ of $\sigma = 0.5\gamma P_{p0}$ and $L_c = 100$ m at $\lambda_s = 1590$ nm was computed while varying the signal output power. The obtained saturation power at $\lambda_s = 1590$ nm, at which the parametric gain was reduced by 3 dB, is at $P_s = -5.61$ dBm, indicated by the vertical dashed line. The saturation power can be further described by power evolution of the pump, signal, and idler [see Fig. 2(b)]. The average output power for each input signal power was obtained based on Eqs. (1)–(3) over a large number of $\delta\beta$ patterns. As observed, in the small-signal regime, the output pump power remains constant. However, the output signal power increased proportionally to the input signal power P_{s0}. This behavior is caused by the power transfer process from the pump to the signal. As a result, the parametric gain in this regime is constant and unsaturated [refer to Fig. 2(a)]. In the saturation regime, on the other hand, the output pump power begins to decrease, and the parametric gain starts to saturate. In this stage, the power is still transferred from the pump to the signal and idler. However, beyond the point where the output pump power is minimum, and output signal power is maximum, the power transfer takes place in the reverse direction, i.e., from the signal and idler to the pump.

The behavior of power evolution and thus the resulting parametric gain is dependent on the position of λ_s. Besides that, the parametric gain is also dependent on β_4[14]. In practice, it is possible to have different fibers with different β_4 but similar β_2 at a particular wavelength. This is because different dispersion profiles associated with different fibers may possibly meet each other at the specific point (the particular wavelength). These profiles have different slopes, and since the slopes are different, β_4 is different as well[20]. Therefore, in order to critically analyze the effect of β_4 on saturation power, the simulations were carried out on three β_4 values, which are $\beta_4 = 0$ (indicates that β_4 is ignored), 3.03×10^{-5}, and 6.23×10^{-5} ps^4/km, while fixing the value of β_2. For each β_4, the position of λ_s was varied.

First, the computation of parametric gain while neglecting β_4, i.e., $\beta_4 = 0$ ps^4/km, was carried out in the small-signal regime of $P_{s0} = -40$ dBm. The results are revealed in Fig. 3(a). It is worth noting that since a total gain spectrum of 1-P FOPA is symmetric with respect to the pump wavelength, here a half-gain spectrum was plotted. As seen, there are two regions that were marked in

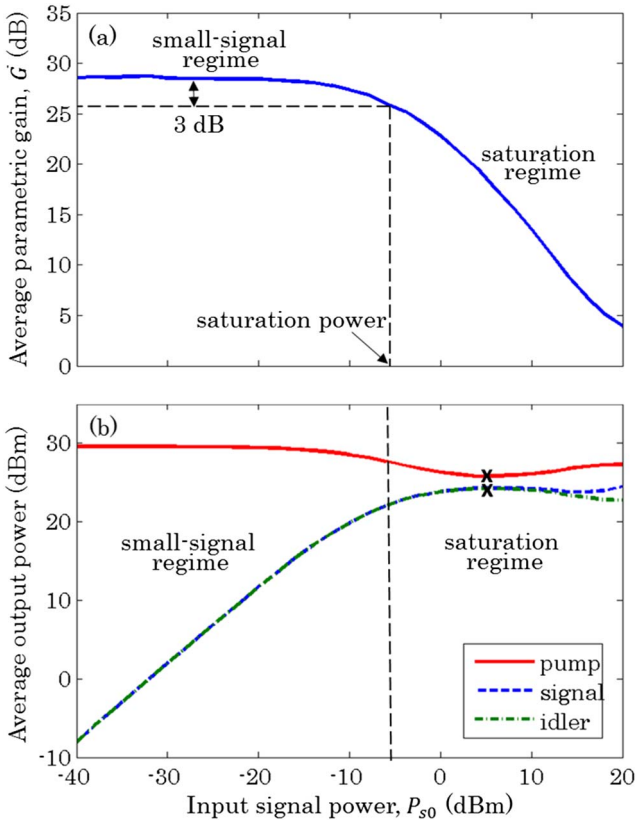

Fig. 2. (a) Saturation curve and (b) average output power at $\lambda_s = 1590$ nm for $\beta_4 = 6.23 \times 10^{-5}$ ps^4/km with fluctuation parameters of $\sigma = 0.5\gamma P_{p0}$ and $L_c = 100$ m.

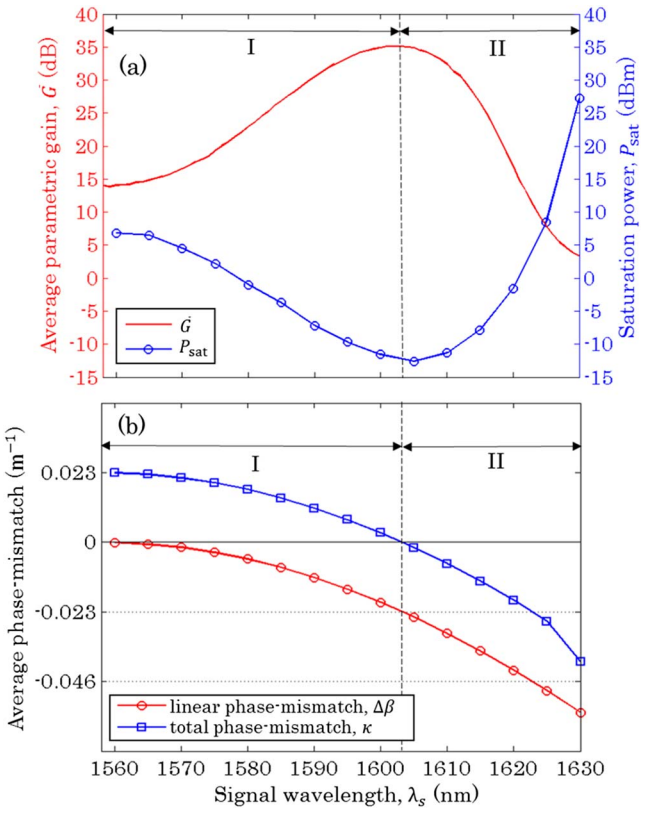

Fig. 3. (a) Half-parametric-gain spectrum for $P_{s0} = -40$ dBm (small-signal regime) and saturation power and (b) phase-mismatch at saturation power with a variation of λ_s for $\beta_4 = 0$ ps^4/km.

Fig. 3(a), i.e., I (1558–1603 nm) and II (1603–1630 nm). In region I, the parametric gain increases as λ_s increases. For example, at $\lambda_s = 1560$ nm, the parametric gain is 14.1 dB, and it increases to 34.9 dB at $\lambda_s = 1600$ nm. This is due to the changes of total phase-mismatch in the fiber [refer to Fig. 3(b)]. Total phase-mismatch is a power dependent function, given as $\kappa = \Delta\beta + \gamma(2P_p - P_s - P_i)$[8]. Perfect phase-matching occurs when $\kappa = 0$, which, in this case, takes place when $\Delta\beta = -\gamma(2P_p - P_s - P_i) \approx -0.023\ \mathrm{m}^{-1}$. As λ_s increases, $\Delta\beta$ reduces and approaches $-0.023\ \mathrm{m}^{-1}$, which then leads to the increase of parametric gain. Basically, the parametric gain at the respective λ_s in the small-signal regime of $P_{s0} = -40$ dBm will affect the corresponding saturation power. This is evidenced by the behavior of saturation power in the same figure, i.e., Fig. 3(a). It can be seen that the higher parametric gain results in lower saturation power. In terms of λ_s, the gain saturates faster (low saturation power) for longer λ_s, at which the parametric gain is higher, if compared to the shorter λ_s, at which the parametric gain is lower. For illustration, the saturation power at $\lambda_s = 1560$ nm is $P_{\mathrm{sat}} = 6.8$ dBm; meanwhile, at $\lambda_s = 1600$ nm, $P_{\mathrm{sat}} = -11.6$ dBm is obtained. At each λ_s, the increment of P_{s0} causes the increase of P_s and P_i [see Fig. 2(b)], thus decreasing the value of nonlinear term $\gamma(2P_p - P_s - P_i)$ of κ. The positive κ then starts to reduce and approaches zero. This means that the efficiency of the amplification process is improved and so is the parametric gain. The longer λ_s does not need higher P_{s0} to reduce the positive κ and make it approach zero, as it already owns a small value of κ (because of $\Delta\beta$ in the small-signal regime). The κ thus tends to depart from zero at the lower P_{s0}, hence leading to the saturation of parametric gain and therefore explaining the reason why parametric gain at longer λ_s saturates faster than that at the shorter λ_s.

Now, as for the parametric gain in region II, in contrast to the behavior in region I, the increase of λ_s causes the parametric gain to reduce. For instance, the parametric gain at $\lambda_s = 1610$ nm is 32.4 dB, but then it reduces to 17.1 dB at $\lambda_s = 1620$ nm. This is because in this region the reduced $\Delta\beta$ starts to depart from $-0.023\ \mathrm{m}^{-1}$, thus reducing the phase-matching condition. Meanwhile, as for the saturation power, the behavior is similar to in region I, i.e., the higher parametric gain results in the lower saturation power. However, in term of λ_s, the gain saturates faster for shorter λ_s (higher parametric gain) if compared to the longer λ_s (lower parametric gain). For example, at $\lambda_s = 1610$ nm, $P_{\mathrm{sat}} = -11.3$ dBm and at $\lambda_s = 1620$ nm, $P_{\mathrm{sat}} = -1.6$ dBm. In this region, the κ value in the small-signal regime at each λ_s is already negative, and the reduction of κ when P_{s0} is increased causes the negative κ to reduce much further away from zero. For this reason, the signal at the longer λ_s reached a lower output level, since the negative κ at longer λ_s is smaller and much further from zero than at the shorter λ_s. This decelerates the power transfer process from the pump to the signal and idler, hence causing the gain saturation to occur at the higher P_{s0}.

Next, the behaviors of parametric gain and saturation power were investigated in presence of β_4, i.e., $\beta_4 = 3.03 \times 10^{-5}\ \mathrm{ps}^4/\mathrm{km}$, with variation of λ_s. First, the parametric gains were calculated with $P_{s0} = -40$ dBm in the presence of dispersion fluctuations, and the results are shown in Fig. 4(a). The analysis is focused on the variation of λ_s in region I (1558–1607 nm), II (1607–1644 nm), III (1644–1670 nm), and IV (1670–1680 nm). Note that the total bandwidth is broader than the previous spectrum in Fig. 3(a), which was without β_4. However, the flatness of the gain spectrum when β_4 exists, particularly when $\beta_4 = 3.03 \times 10^{-5}\ \mathrm{ps}^4/\mathrm{km}$, is poor. In regions I and II, the behaviors of parametric gain and saturation power are similar with the behavior in Fig. 3(a). This is because in these two regions the effect of β_4 is not significant, which is due to the small value of $\omega_p - \omega_s$ in Eq. (4). The reduction of parametric gain and the increase of saturation power in region II, however, are not continuous. As in region III, the parametric gain starts to climb back; meanwhile, the saturation power begins to fall back on. This is because in region III the term of $\omega_p - \omega_s$ is considered large enough to significantly affect β_4. The positive value of β_4 begins to counteract the negative value of β_2 in Eq. (4), hence increasing the negative $\Delta\beta$. Consequently, negative κ increases and approaches zero again, thus increasing the parametric gain. Meanwhile, the reason for saturation power behavior over the increase of λ_s in

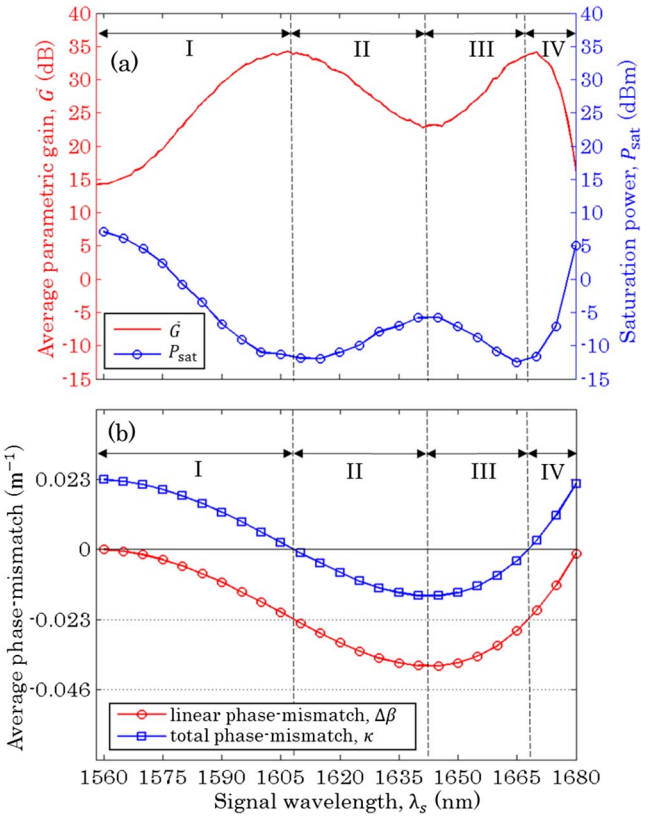

Fig. 4. (a) Half-parametric-gain spectrum for $P_{s0} = -40$ dBm (small-signal regime) and saturation power and (b) phase-mismatch at saturation power with a variation of λ_s for $\beta_4 = 3.03 \times 10^{-5}\ \mathrm{ps}^4/\mathrm{km}$.

region III is similar to the behavior in region I, when β_4 is ignored (Fig. 3), except the case that κ approaches zero from the negative regime. The approach of κ back to zero after its departure in region II is obviously related to the changes of $\Delta\beta$ after the value of β_4 starts to be significant. Hence, for this reason, the parametric gain is increased, and saturation power is decreased. Now, in region IV, the parametric gain reduces, and, at the same time, the saturation power is increased over the increment of λ_s. Unfortunately, the increase of negative κ in region III will eventually lead to the positive value of κ, which means it will depart from zero, cause the parametric gain to reduce again, and hence increase the saturation power, which is similar to region II.

Based on the report in Ref. [10], the flatness of the gain spectrum can be enhanced when a fiber with high β_4 was used as a gain medium of the 1-P FOPA. Therefore, this time the parametric gain and saturation power were investigated with $\beta_4 = 6.23 \times 10^{-5}$ ps^4/km, while the other parameters were fixed as the previous. The results are shown in Fig. 5(a). Roughly, it can be observed that the behaviors of parametric gain and saturation power in regions I (1558–1615 nm) and II (1615–1645 nm) are similar to the behavior in Fig. 3(a). Although their gain behaviors are similar, the phase-mismatch in the fiber with and without β_4 is different. This is because the

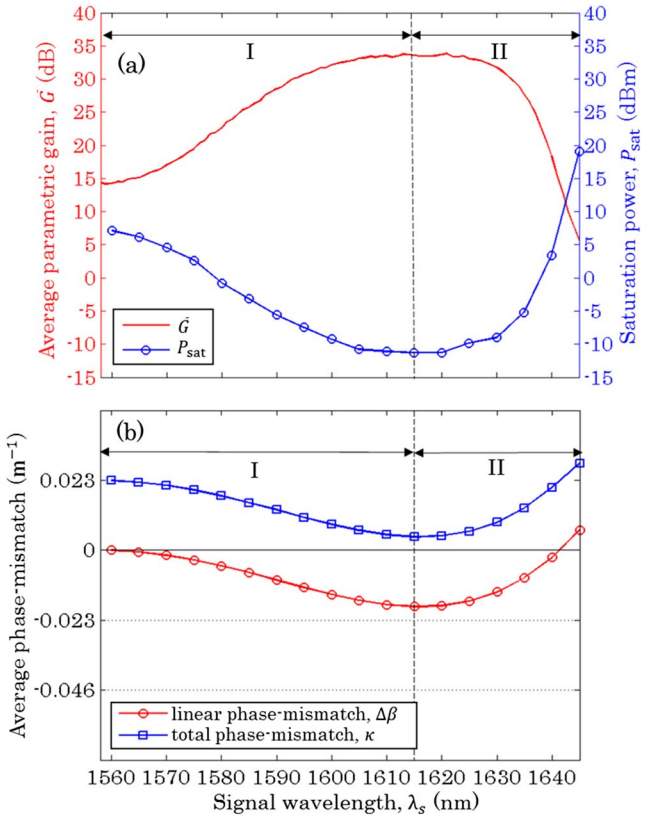

Fig. 5. (a) Half-parametric-gain spectrum for $P_{s0} = -40$ dBm (small-signal regime) and saturation power and (b) phase-mismatch at saturation power with a variation of λ_s for $\beta_4 = 6.23 \times 10^{-5}$ ps^4/km.

further increment of $\omega_p - \omega_s$ value in Eq. (4) does not cause the κ to fall to a negative value. This is due to the increment that caused the β_4 value to be significant. The positive value of β_4 starts to counteract the negative value of β_2. Consequently, the previous decreasing $\Delta\beta$ begins to increase, consequently increasing the κ and causing it to depart from zero. This then causes the reduction of parametric gain and the increase of saturation power with the increasing λ_s in regime II. The behavior of phase-mismatch has optimized the performance of parametric gain and, thus, enhanced the flatness of the gain spectrum. Based on the saturation power behavior of all β_4 values, it shows that the saturation powers at a particular λ_s are different. For instance, at $\lambda_s = 1625$ nm, $P_{sat} = 8.4$, -10, and -9.8 dBm for $\beta_4 = 0$, 3.03×10^{-5}, and 6.23×10^{-5} ps^4/km, respectively. This clearly proves that the value of saturation power at a particular λ_s and, thus, the saturation power behavior over the entire signal wavelength span are dependent on the higher-order dispersion coefficients of the optical fiber.

All in all, the performance of the 1-P FOPA, particularly the parametric gain and saturation power while varying the λ_s, was investigated in this work. The behaviors of respective performance parameters were critically analyzed on three different values of β_4 in the presence of random dispersion fluctuations. The Runge–Kutta–Fehlberg method was used to solve the three-coupled amplitude equations. Generally, the behaviors of the performance parameters at each λ_s are contrary to each other. The higher parametric gain leads to the lower saturation power and vice versa. As the phase-matching condition is implicitly dependent on λ_s, the manipulation of λ_s would affect the efficiency of the phase-matching condition and, thus, the 1-P FOPA performance. The efficiency of the phase-matching condition is not only reliant on λ_s, but also on β_4. The higher value of β_4 optimized the parametric gain performance while enhancing the flatness of the gain spectrum. Since the saturation power is dependent on the parametric gain, it means that the presence of β_4 is vital in analyzing and tailoring the saturation power at a particular λ_s, especially at longer λ_s.

This work was supported by the Fundamental Research Grant Scheme (FRGS) vot K095 granted by Ministry of Education (MOE) Malaysia.

References

1. G. Agrawal, *Nonlinear Fiber Optics* (Elsevier, 2007).
2. N. A. Cholan, M. H. Al-Mansoori, A. S. M. Noor, A. Ismail, and M. A. Mahdi, Opt. Express **21**, 6131 (2013).
3. N. S. Mohd Shah and M. Matsumoto, Opt. Commun. **284**, 4687 (2011).
4. O. F. Anjum, M. Guasoni, P. Horak, Y. Jung, P. Petropoulos, and D. J. Richardson, J. Light. Technol. **36**, 3678 (2018).
5. M. E. Marhic, P. A. Andrekson, P. Petropoulos, S. Radic, C. Peucheret, and M. Jazayerifar, Laser Photon. Rev. **9**, 50 (2015).
6. M. E. Marhic, *Fiber Optical Parametric Amplifiers, Oscillators and Related Devices* (Cambridge University, 2007).
7. G. Keiser, *Optical Fiber Communication* (McGraw Hill, 2015).

8. K. Inoue and T. Mukai, Opt. Lett. **26**, 10 (2001).
9. M. Bagheri, H. Pakarzadeh, and A. Keshavarz, Appl. Opt. **55**, 3368 (2016).
10. N. Othman, N. S. Mohd Shah, K. G. Tay, H. Pakarzadeh, and N. A. Cholan, Appl. Opt. **56**, 29 (2017).
11. T. Kazama, T. Umeki, M. Abe, K. Enbutsu, Y. Miyamoto, and H. Takenouchi, J. Lightwave Technol. **35**, 755 (2017).
12. H. Wang, F. Li, and Y. Ji, Opt. Eng. **56**, 026101 (2017).
13. H. Pakarzadeh and A. Zakery, Opt. Commun. **309**, 30 (2013).
14. M. E. Marhic, N. Kagi, T. K. Chiang, and L. G. Kazovsky, Opt. Lett. **21**, 573 (1996).
15. M. Hirano, T. Nakanishi, and M. Onishi, IEEE J. Sel. Top. Quantum Electron. **15**, 103 (2009).
16. J. Hansryd, P. A. Andrekson, M. Westlund, J. Li, and P. O. Hedekvist, IEEE J. Sel. Top. Quantum Electron. **8**, 506 (2002).
17. M. Farahmand and M. de Sterke, Opt. Express **12**, 136 (2004).
18. S. K. Chatterjee, S. N. Khan, and P. R. Chaudhuri, Opt. Commun. **332**, 244 (2014).
19. K. G. Tay, N. Othman, N. S. M. Shah, and N. A. Cholan, Telkomnika **15**, 3 (2017).
20. N. Othman, N. S. M. Shahida, K. G. Tay, H. Pakarzadeh, N. A. Cholan, and R. Talib, AIP Conf. Proc. **1883**, 020008 (2017).